AGU PUBLICATIONS

JGR

Journal of Geophysical Research: Oceans

RESEARCH ARTICLE

10.1002/2014JC010194

Key Points:
- Uncertainty estimate to the OAFlux vector wind analysis is analyzed
- An ensemble error perturbation approach is used to estimate the uncertainty
- High winds and rain are shown to be the leading sources of uncertainty

Correspondence to:
L. Yu,
lyu@whoi.edu

Citation:
Yu, L., and X. Jin (2014), Confidence and sensitivity study of the OAFlux multisensor synthesis of the global ocean surface vector wind from 1987 onward, *J. Geophys. Res. Oceans*, *119*, 6842–6862, doi:10.1002/2014JC010194.

Received 29 MAY 2014
Accepted 16 SEP 2014
Accepted article online 19 SEP 2014
Published online 15 OCT 2014

Confidence and sensitivity study of the OAFlux multisensor synthesis of the global ocean surface vector wind from 1987 onward

Lisan Yu[1] and Xiangze Jin[1]

[1]Woods Hole Oceanographic Institution, Woods Hole, Massachusetts, USA

Abstract This study presented an uncertainty assessment of the high-resolution global analysis of daily-mean ocean-surface vector winds (1987 onward) by the Objectively Analyzed air-sea Fluxes (OAFlux) project. The time series was synthesized from multiple satellite sensors using a variational approach to find a best fit to input data in a weighted least-squares cost function. The variational framework requires the a priori specification of the weights, or equivalently, the error covariances of input data, which are seldom known. Two key issues were investigated. The first issue examined the specification of the weights for the OAFlux synthesis. This was achieved by designing a set of weight-varying experiments and applying the criteria requiring that the chosen weights should make the best-fit of the cost function be optimal with regard to both input satellite observations and the independent wind time series measurements at 126 buoy locations. The weights thus determined represent an approximation to the error covariances, which inevitably contain a degree of uncertainty. Hence, the second issue addressed the sensitivity of the OAFlux synthesis to the uncertainty in the weight assignments. Weight perturbation experiments were conducted and ensemble statistics were used to estimate the sensitivity. The study showed that the leading sources of uncertainty for the weight selection are high winds (>15 ms^{-1}) and heavy rain, which are the conditions that cause divergence in wind retrievals from different sensors. Future technical advancement made in wind retrieval algorithms would be key to further improvement of the multisensory synthesis in events of severe storms.

1. Introduction and Background

A high-resolution global analysis of daily-mean ocean-surface vector winds from 1987 onward has been recently developed by the Objectively Analyzed air-sea Fluxes (OAFlux) project through objective synthesis of 12 satellite wind sensors [*Yu and Jin*, 2014; hereafter YJ14]. The 12 satellite sensors include 2 scatterometers that have wind speed and direction retrievals and 10 passive microwave radiometers that have wind speed retrievals only. The two scatterometers include the SeaWind scatterometer on the NASA's QuikSCAT mission (June 1999 to November 2009) and the Advanced Scatterometer (ASCAT) onboard the MetOp–A satellite (October 2006 onward) launched by the European Organisation for the Exploitation of Meteorological Satellites (EUMETSAT). The 10 passive radiometers include six sensors (F08, F10, F11, F13, F14, and F15) from the Special Sensor Microwave Imager (SSM/I) aboard Defense Meteorological Satellite Program (DMSP) satellites (July 1987 onward), two sensors (F16 and F17) from the DMSP's Special Sensor Microwave Imager/Sounder (SSMIS) (November 2005 onward), and one passive polarimetric microwave radiometer that was launched aboard the joint Department of Defense (DoD)/Navy platform Coriolis mission in January 2003.

The variational approach in use was developed from the theory of least-variance linear statistical estimation [*Lorenc*, 1988; *Daley*, 1991; *Talagrand*, 1997], in which the estimates of the wind speed (w), and the zonal (u) and meridional (v) wind components were obtained by finding a best fit to input data (satellite observations, reanalysis wind components, and a priori terms) in a weighted least-squares cost function. Two a priori conditions were imposed in the cost function. One is that the analyzed wind speed $w=sqrt(u^2+v^2)$ needs to be as close as possible to satellite wind speed retrievals, and the other is that the analyzed (u,v) needs to satisfy the kinematic constraints such as vorticity and divergence conservations. Surface vector winds from two atmospheric reanalyses served as the background information for u and v. The two reanalysis wind products were the European Centre for Medium-Range Weather Forecasts (ECMWF) Re-Analysis (ERA)

interim (hereafter ERA-Interim) project [*Dee et al*., 2011] and the Climate Forecast System Reanalysis (CFSR) from the National Centers for Environmental Prediction (NCEP) [*Saha et al*., 2010]. These two reanalyses have improved characterization of the global ocean surface winds compared with other reanalysis wind products when validated with buoy measurements [e.g., *Yu and Jin*, 2012].

One prerequisite for all applications based on the least-variance linear statistical estimation theory is the a priori specification of the weight (i.e., an inversion of error covariance) for each data set used in the cost function so that the errors in data can be accounted for during the search of a solution [*Talagrand*, 1999]. In reality, those error statistics can neither be perfectly known nor be accurately specified, rendering the optimality of such framework to be dependent on the ability to obtain the most appropriate representation of error statistics [*Courtier et al*., 1994; *Wahba et al*., 1995; *Desrozier and Ivanov*, 2001]. Two questions were thus raised for the OAFlux vector wind analysis. One is how to provide the best possible weight assignments for all the input data, and the other is how to quantify the degree of uncertainty in the resultant vector wind estimates caused by the uncertainty in the weight assignments. These two issues are to be addressed here, aiming to providing confidence and sensitivity analysis to the newly developed OAFlux vector wind time series and to complementing the study of YJ14.

Extensive efforts have been made to identify, characterize, and quantify the errors in satellite wind measurements using a variety of reference platforms, including in situ buoys, research vessels, and atmospheric reanalyses [e.g., *Ebuchi et al*., 2002; *Bourassa et al*., 2003; *Vogelzang et al*., 2011]. There are two general sources of error in satellite observations. One is measuring instrumentation noise that results from random errors of the observing system [e.g., *Kent and Challenor*, 2006]. For scatterometer retrievals, ambiguity selection errors are regarded as measurement errors [e.g., *Hoffman*, 1984; *Freilich*, 1997; *Stoffelen*, 1998; *Bourassa et al*., 2003]. The other is representation errors [e.g., *Stoffelen*, 1998; *Schlax et al*., 2001; *Kent and Kaplan*, 2006; *Bourassa and Ford*, 2010; *Vogelzang et al*., 2011; *Fangohr and Kent*, 2012], including errors that are associated with unresolved spatial/temporal scales, errors due to the approximations in the geophysical model functions (GMF) that relate backscatter to wind vector, and/or those approximations in radiative transfer models (RTM) that relates emissivity to wind speed. The representation of the wind retrievals at high wind speeds is one example of the representation errors. The presently large uncertainties in high wind retrievals are attributable to the lack of high wind measurements from buoys or research vessels to validate the empirical assumptions in the GMFs and/or RTMs [e.g., *Fangohr and Kent*, 2012; *Yueh et al*., 2001]. Rain is another source of bias for the Ku-band scatterometer retrievals. Removing the rain-contaminated wind vector cells in QuikSCAT can lead to a large-scale bias in wind derivative fields [e.g., *Milliff et al*., 2004], which elucidates a fact that the representation errors can have both a bias component and a random component [e.g., *Bourassa and Ford*, 2010].

Representation errors together with measurement errors constitute the error covariances for data constraints. However, two additional sources of error need to be considered when estimating the cost function that included not only 12 different sensors but also atmospheric reanalyses as the background fields. One error source is the model errors (biases) in the atmospheric reanalyses, and the other is the interpolation or mapping error that arises when merging satellite measurements made at discrete times onto the selected temporal resolution of equal interval. For instance, each sensor provides two daily passes, one as the orbit ascends and the other as the orbit descends. As the number of available sensors (and so the total daily passes) changes constantly with time (see Figure 1 in YJ14) from 1987 to the present, the underrepresentation of subdaily variability in the resultant daily-mean synthesis could be a source of error.

In YJ14, we reported that the most challenging situation for the OAFlux synthesis is the construction of the near-surface circulation associated with synoptic weather storms that feature high winds (>15 ms^{-1}) correlated with rain conditions. Five factors contribute to the challenge. One is the lack of passive microwave radiometer wind speed retrievals in rain conditions, which reduces satellite data coverage for the synoptic weather systems. The second is that the removal of the rain contaminated wind vector cells in QuikSCAT creates data voids that cannot be easily filled by the reanalysis winds because of the smooth spatial variability in the latter. It is worth noting, however, a new QuikSCAT product was recently developed by *Fore et al*. [2014], in which a neural network approach was implemented to correct rain contaminated wind speeds rather than to flag them out [*Ricciardulli and Wentz*, 2011]. Work is underway to examine the likely improvement of the OAFlux vector wind estimates under rain by utilizing this new rain-corrected QuikSCAT product. The third factor is that there are differences between wind retrievals from the C-band ASCAT [*ASCAT Wind Product User*

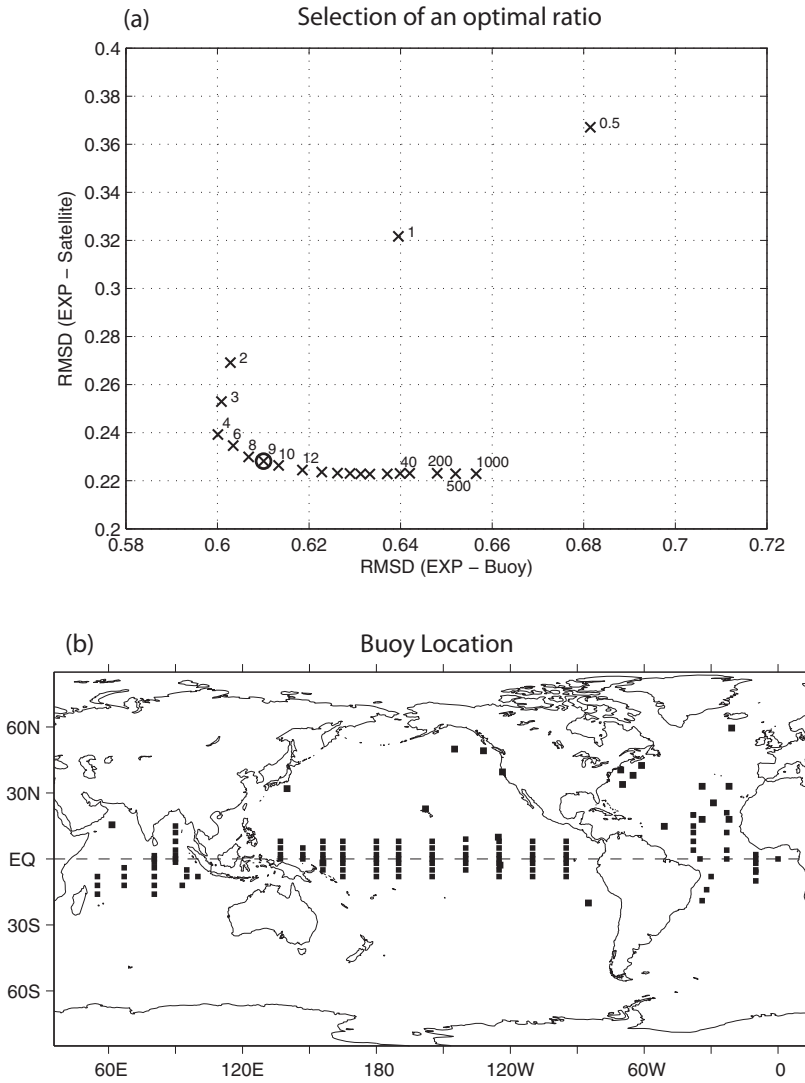

Figure 1. (a) Selection of the optimal weight ratio based on two criteria, namely, the STD wind speed differences between the minimum of the cost function and buoy measurements (*x* axis) and the STD wind speed differences between the minimum of the cost function and input satellite observations (*y* axis). Each cross represents one experiment, with the corresponding weight ratio marked next to the cross. (b) Location of buoys used in the weight selection experiment.

Manual, 2013] and the Ku-band QuikSCAT [*Ricciardulli and Wentz*, 2011] at high winds (>15 ms^{-1}) due primarily to the lack of in situ buoy validation of the GMFs at high-wind conditions [e.g., *Dunbar et al.*, 2006; *Fangohr and Kent*, 2012; *Kent and Challenor*, 2006; *Kent and Kaplan*, 2006; *Bentamy et al.*, 2012]. The sensitivity experiments in YJ14 showed that the interscatterometer differences are a source of representation error for the synthesis. The fourth factor is that high winds generally correspond to fast transient changes and thus a few instantaneous samples over a day will not accurately determine the mean wind over a day at these locations. The fifth factor is that rain corresponds to moist convection, particularly in the tropics, which is associated with hourly rather than daily time scales of wind changes.

The objective approach in use is statistically based, which is not expected to mitigate the impacts of missing or biased satellite wind retrievals in events of severe rainy storms. This approach is capable of reducing random errors (noises) in the given retrievals and searching for a solution that best fits the data constraints and the a priori information within the predescribed weights. It is, however, unable to generate an improved estimate in the presence of missing or biased retrievals, and unable to remove the biases associated with representation errors due to either satellite observations, or atmospheric reanalysis winds, or mapping. The objective synthesis is subject to the specification of error statistics (or weights) for both

random and representation components. Nevertheless, despite the extensive progresses that have been achieved in understanding and quantifying the representation errors of satellite and reanalysis winds [e.g., *Stoffelem*, 1998; *Ebuchi et al*., 2002; *Bourassa et al*., 2003; *Vogelzang et al*., 2011; *Yu and Jin*, 2012] and in employing a bias correction scheme to data assimilation to reduce the effect of biases on atmospheric reanalysis [e.g., *Desroziers and Ivanov*, 2001; *Dee*, 2005], not all error sources are well estimated. For example, it is usually assumed that the errors between sensor themselves and between the sensors and atmospheric reanalyses are uncorrelated. In reality, sensors are calibrated against each other [e.g., *Stoffelen and Anderson*, *1997*; *Ricciardulli and Wentz*, 2011], and ERA-interim and CFSR both assimilate scatterometer observations [e.g., *Dee et al*., 2011; *Saha et al*., 2010]. Hence, the errors that directly depend on the observation inputs are not accounted for. The multisensor synthesis is prone to so many sources of error that no matter what the weights are assigned, there is always a degree of uncertainty in the assignment, which consequently affects the best fit of the cost function.

We present here our efforts in seeking (i) a practical use of existing buoy observations for assigning weights and (ii) a feasible representation of the uncertainty in the weight assignments and the subsequent impact on the resultant vector wind analysis. We designed a weight-selection experiment to find the weights that make the minimum of the cost function to be as close as possible to not only input satellite observations but also in situ buoy measurements at 126 locations that were not the input of the synthesis (section 2). We further designed an ensemble-based weight perturbation experiment to generate an ensemble of the solutions in response to randomized weights and to use the ensemble statistics as a measure of the uncertainty of the solution due to the uncertainty of the weight assignment (section 3). The results showed that the leading sources of uncertainty in the OAFlux wind analysis are the high winds and rain conditions, which are summarized and discussed in section 4. Nevertheless, the sources of error in the input satellite and also background reanalysis data sets are complex and often intercorrelated, which have been shown in the excises of the 3-D-VAR or 4-D-VAR data assimilation for the numerical weather prediction system [e.g., *Wahba et al*., 1995; *Courtier et al*., 1998] and the variational approach for producing gridded products from blending various observations [*Legler et al*., 1989; *Hoffman et al*., 2003; *Atlas et al*., 2011; *Yu and Jin*, 2014]. A realistic definition of the error covariance matrices, and hence the weights, remains as a matter of permanent and various efforts for all applications of least-variance linear statistical estimation [*Dee*, 2005; *Sadiki and Fisher*, 2005; *Bannister*, 2007]. This study represents our first step toward establishing a framework for systematic error modeling for the vector wind analysis using least-variance linear statistical estimation.

2. The Weight Selection Experiments

2.1. The Cost Function

As described in YJ14, the cost function formulated for the OAFlux multisensor synthesis is expressed as follows:

$$F = \underbrace{\frac{1}{2}(\vec{V}_a-\vec{V}_b)^T R_b\left(\vec{V}_a-\vec{V}_b\right)}_{(\mathrm{I})} + \underbrace{\frac{1}{2}(\vec{V}_a-\vec{V}_o)^T R_o\left(\vec{V}_a-\vec{V}_o\right)}_{(\mathrm{II})} + \underbrace{\frac{1}{2}(w_a-w_o)^T S_o(w_a-w_o)}_{(\mathrm{III})} + \underbrace{\gamma(\nabla\times\vec{V}_a-\nabla\times\vec{V}_b)^2}_{(\mathrm{IV})} + \underbrace{\lambda(\nabla\cdot\vec{V}_a-\nabla\cdot\vec{V}_b)^2}_{(\mathrm{V})} \quad (1)$$

where $\vec{V}=(u,v)$ is wind vector with zonal and meridional wind components denoted as u and v, respectively, and $w=\sqrt{u^2+v^2}$ is wind speed. The superscript "T" denotes transpose. There are three subscripts: "a" denotes an estimate, "b" the background fields, and "o" satellite observations. The matrices R_b, R_o, and S_o are weighting matrices that theoretically are inversely proportional to the respective error covariance matrices of the background wind vector fields ($\vec{V}_b$), satellite wind vector observations ($\vec{V}_o$), and satellite wind speed observations (w_o). The parameters, γ and λ, are the scalings that control the effectiveness of the vorticity and divergence constraints.

The first three terms (I)-(III) are data constraints that represent a least-squares fitting of the analyzed zonal wind, meridional wind, and wind speed to input background and satellite data sets. The input satellite observations included SSM/I F08, F10, F11, F13, F15, SSMIS F16, F17, AMSRE, WindSat, QuikSCAT, and ASCAT. Among the 12 sensors, QuikSCAT and ASCAT have observations of zonal and meridional wind components

while all others are radiometers providing only wind speed observations. The wind direction retrievals from WindSat were not included due to large uncertainties when compared to buoy measurements and QuikSCAT [*Yu and Jin*, 2012]. The background fields were taken from ERA-Interim and CFSR, which provided information for (i) initializing wind direction when there are no scatterometer measurements prior to 1999, and (ii) gap-filling in regions where there are no satellite observations. The two reanalysis winds were also the background fields for the fourth and fifth terms (IV)-(V), which are the weak constraints for the vorticity and divergence. These two kinematic terms are spatial derivative constraints, which are used mainly for suppressing the jumps in satellite observations at the swath edges. These jumps at the swath edges are not caused by the instrument error but by the discontinuity between measurements made at different times of day. The jumps are particularly acute in case of fast moving storms. The contribution of these kinematic terms to the minimization process is prescribed by the scaling parameters γ and λ. Readers are referred to YJ14 for the description of satellite sensors, download data sources, and the synthesis procedure.

The minimization process seeks an estimate of daily wind field of *u*, *v*, and *w* that satisfies the data constraints and the imposed kinematic constraints within the specified weights by using a conjugate-gradient iterative method [*Yu et al*., 2008]. As described in Introduction, the main challenge for estimating the cost function (1) is the specification of the weight (i.e., an inversion of error covariance matrix) for each data set [e.g., *Courtier et al*., 1994; *Wahba et al*., 1995; *Desrozier and Ivanov*, 2001]. The errors in input satellite and reanalysis data sets have both random and systematic components. The variational approaches are capable of reducing the random errors (noises) but not the biases [*Talagrand*, 1999]. Many efforts have been made to develop bias-aware weight correction methods [e.g., *Stoffelen*, 1998; *Harris and Kelly*, 2001; *Dee*, 2005] that can estimate and correct systematic errors jointly with the variable estimates. These methods require an accurate attribution of the detected bias to its source in order to develop useful representations for the biases or the mechanisms that cause the biases to occur. However, the separation of biases into various sources requires additional information (such as independent observations, knowledge of the underlying causes, and/or hypotheses about the error characteristics of possible sources). One major drawback is that the bias-aware correction methods may not produce the right correction if several sources have the similar bias pattern but there is no sufficient information to separate the sources [e.g., *Chapnik et al*., 2004; *Desroziers et al*., 2005; *Dee*, 2005].

In addition to the random errors and the biases in input satellite and reanalysis winds, error correlations between satellites and reanalyses winds are also evidenced [e.g., *Stoffelen*, 1998; *Frehlich*, 2011; *Vogelzang et al*., 2011; *Vogelzang and Stoffelen*, 2012; *Bonavita*, 2012]. Needless to say, we do not have sufficient information to formulate an accurate representation for all types of errors. In this study, the strategy is simple, which is to start from scratch and construct the basic errors. The goal is straightforward, which is to develop a framework that allows an identification of the uncertainty in the weight assignment and a quantification of the effect of the weigh-assignment errors on the resultant vector wind analysis.

2.2. Design of the Weight Selection Experiments

Assuming that the errors are constant and uncorrelated, the cost function (1) can be simplified as follows:

$$F=\frac{1}{2}\sum_{i=1}^{I}\alpha_i(u_a-u_i)^2+\frac{1}{2}\sum_{i=1}^{I}\alpha_i(v_a-v_i)^2+\frac{1}{2}\sum_{j=1}^{J}\beta_j\left(w_a-w_j\right)^2+\gamma(\nabla\times\vec{V}_a-\nabla\times\vec{V}_b)^2 \\ +\lambda(\nabla\cdot\vec{V}_a-\nabla\cdot\vec{V}_b)^2 \tag{2}$$

where α_i represents the weight assignment for zonal and meridional wind components, with the subscript $i = 1, \ldots, I$ indicating the respective input scatterometers (i.e., QuikSCAT and ASCAT) and background (i.e., ERA-interim and CFSR) data sets for wind components. The weight assignment for the wind speed term is denoted by β_j, with the subscript $J = 1, \ldots, J$ indicating the respective input satellite wind speed data sets (e.g., SSM/I F08, F10, F11, F13, F15, SSMIS F16, F17, AMSR-E, WindSat, QuikSCAT, and ASCAT).

In YJ14, we indicated that the weights, β_j, associated with the wind speed constraints (term (III)), were set to be 1. The weights of the ERA-interim *u* and *v* terms were assigned to be 0.8 and those of CFSR were set to be 0.4. The scaling parameters of the kinematic constraints for vorticity and divergence, γ and λ, were fixed at 0.5. The values of these weight parameters were selected from numerous sensitivity experiments that can be explained using Figures 1a and 1b. In essence, the weights were selected from the experiments

based on the criterion (Figure1a) that the chosen weights should make the cost minimum closest to both input satellite data sets and the air-sea buoy measurements at 126 locations [*Yu and Jin*, 2012]. The buoy measurements (Figure 1b) were not included in estimating the cost function (2), although most of them were assimilated by reanalyses [e.g., *Dee et al*., 2011 and *Saha et al*., 2010]. These buoy measurements may be best regarded as a quasi-independent reference. In designing the weight selection experiments, we utilized the fact that, once errors are assumed to be constant, the minimization of the cost function (2) depends on the relative values, or the ratio, between the weights assigned to the satellites and the weights to the reanalyses. Furthermore, we assigned an equal weight to the satellite sensors, as their statistics with regard to the 126 buoy time series were highly comparable [*Yu and Jin*, 2012]. Finally, we kept the ratio between the total weights for the satellite data constraints and the total weights for the reanalyses constraint to remain unchanged during the analysis period. Hence, it is the weight ratio that was determined from the weight selection experiments. There are 11 satellite observation constraints (i.e., seven satellite wind speed constraints, two scatterometer zonal wind constraints, and two for scatterometer meridional wind constraints) and 4 reanalysis constraints for zonal and meridional wind components. After setting an equal weight to all satellite constraints, the weight ratio can be calculated as κ = total weights for satellite constraints/total weights for reanalysis constraints = 11/*x*, where x denotes the total weights for reanalysis constraints and can be determined once the optimal κ is selected.

2.3. Results

The statistical behavior of the weight selection experiments is plotted (Figure 1a) using two measures, the wind speed root-mean square differences (RMSD) between the experiments and buoys (the *x* axis) and the wind speed RMSD between the experiments and seven satellite sensors (i.e., SSM/I F13, SSMIS F16, F17, AMSR-E, QuikSCAT, ASCAT, and WindSat) (*y* axis). A total of 200 experiments were conducted for the year 2008 to test the performance of the cost function in response to the weight ratio that ranges from 0.5 to 1000 (i.e., the range of the total weights assigned to the reanalysis constraints varies from 22 to 0.01). The larger (smaller) the weight ratio, the more dominant the satellite (reanalysis) data constraints are on the minimization of the cost function. As can be seen in Figure 1a, the wind speed RMSD with respect to the satellites (the *y* axis) reaches a steady state value of 0.22 ms^{-1} once the weight ratio increases beyond 15. However, the larger the weight ratio, the farther the experiments depart away from the buoy-based RMSD (the *x* axis). The smallest RMSD with buoy is 0.6 ms^{-1} when the weight ratio is at 4. The two measures when combined suggests that an optimal weight ratio should be between 4 and 15, upon which we decided to choose κ=9. This says that the corresponding total weights for the reanalysis constraints, *x*, is 1.2 when the total weights for the satellite constraints are set at 11. Similar experiments were conducted to decide the partition between ERA-interim (i.e., 0.8) and CFSR (i.e., 0.4) and also to determine the scaling parameters (i.e., both set at 0.4) of the kinematic constraints to the minimization of the cost function (not shown).

Talagrand [1999] discussed the usefulness of the statistics of the differences between the minimum of the cost function and input observations (i.e., the so-called innovation vector) in a posteriori diagnostics of the estimation system. His work laid an important framework for *Desrozier and Ivanov* [2001] to develop an adaptive tuning of the error covariance parameters for the variational estimation. Our study here demonstrates that the innovation vectors can be combined with the buoy measurements to help select the optimal weights needed by the cost function.

3. The Ensemble-Based Weight Perturbation Analysis

3.1. Design of the Ensemble-Based Weight Perturbation Experiment

The weights that were determined from the weight selection experiments represent an estimate and hence, have a degree of uncertainty. As the solution of the variational estimation depends on the weights, there is a need to identify the pattern of the uncertainty and to characterize and quantify the effect of the uncertainty on the resultant vector wind analysis. To do so, we designed an uncertainty analysis that relies on a randomization of weights to generate an ensemble of perturbed analyses. The idea is spiritually similar to the ensemble assimilation that has been commonly used in numerical weather prediction centers to improve the estimation of error statistics associated with the model forecasts and the observations [e.g., *Houtekamer et al*., 1996; *Fisher*, 2003; *Buehner et al*., 2005; *Berre et al*., 2006; *Frehlich*, 2011; *Bonavita et al.,* 2012]. In particular, *Desroziers and Ivanov* [2001] and *Chapnik et al*. [2004] proposed a randomization

approach that generates an ensemble of perturbed analyses by perturbing the observations to allow for a posteriori tuning of the error covariances using the ensemble statistics of the perturbed analyses. Our perturbation approach differs from that of ensemble data assimilation in two major ways. First, we perturb the weights, not the observations [*Evensen*, 1994]. Second, we use the ensemble statistics of the perturbed analyses to determine the degree of the uncertainty of the OAFlux analysis, unlike the ensemble assimilation that uses the ensemble statistics to improve the weight assignments [e.g., *Houtekamer et al*., 1996; *Sadiki and Fisher*, 2005; *Desroziers et al*., 2009].

The idea of the weight perturbation experiments stem from the fact that if the weights are not known exactly and have to be assigned, then the solution obtained from the minimization process cannot be unique. Hence, there will be N sets of solutions when N sets of weight assignments are given, and the statistics of the ensemble with N members can provide an uncertainty estimate to the solution of the cost function. In randomizing the weights for the N sets of experiments, one condition is enforced, that is, the sum of all the weights for each experiment is equal to one:

$$\sum_{i=1}^{I}\alpha_i+\sum_{j=1}^{J}\beta_j=1 \tag{3}$$

The weak constraints in the cost function (2) (i.e., terms (IV) and (V)) are secondary constraints that are imposed to suppress the noises in satellite observations at the swath edges, while the uncertainty in the weight assignments associated with the data constraints (i.e., terms (I)–(III)) are the leading contributors to the uncertainty of the variational estimation. By focusing on the first three terms in (2), an analytic solution for w_a, u_a, and v_a that minimizes the cost function F can be derived as follows:

$$w_a=\sum_{j=1}^{J}\beta_j w_j+\sqrt{\left(\sum_{i=1}^{I}\alpha_i u_i\right)^2+\left(\sum_{i=1}^{I}\alpha_i v_i\right)^2} \tag{4}$$

$$u_a=\sum_{i=1}^{I}\alpha_i u_i\Big/\left(1-\frac{1}{w_a}\sum_{j=1}^{J}\beta_j w_j\right) \tag{5}$$

$$v_a=\sum_{i=1}^{I}\alpha_i v_i\Big/\left(1-\frac{1}{w_a}\sum_{j=1}^{J}\beta_j w_j\right) \tag{6}$$

where the dependence of w_a, u_a, and v_a on input data sets w_i, u_i, and v_j, as well as on weights α_i and β_j, is established. Once the N sets of weight assignments are generated by randomization, the resultant N sets of the solution for w_a, u_a, and v_a can then be used to assess the uncertainty of w_a, u_a, and v_a associated with the weight assignment errors. Here, the uncertainties of w_a, u_a, and v_a are expressed in terms of the standard deviation (STD):

$$\sigma_W=STD\left(w_{a,n}\right) \tag{7a}$$

$$\sigma_u=STD\left(u_{a,n}\right) \tag{7b}$$

$$\sigma_v=STD\left(v_{a,n}\right) \tag{7c}$$

where $n = 1,\ldots N$, denoting the N sets of the solution corresponding to N sets of weight assignments.

To examine how many weight perturbation experiments are needed, we first tested N from 1 to 160. The change of the globally averaged σ_w, σ_u, and σ_v with respect to the number of experiments was shown for the year 2008 (Figure 2), indicating that the ensemble statistics come to a quasi steady state when N is around 40. Further increase of N does not alter the statistics, because the degree of freedom for errors is determined by the number of input data sets rather than the number of experiments. In the following analysis, the σ_w, σ_u, and σ_v computed at N=40 are used, and these errors are referred to as the STD of *w, u, v* associated with the uncertainty in weight assignments (equations (7a–c)).

3.2. Deriving the Uncertainty in Wind Stress and Components

Once the uncertainties in wind speed, zonal and meridional components are determined, the uncertainties in wind stress, τ, zonal and meridional stress components, τ_x and τ_y, can be readily derived from the error

propagation theory. The wind stress is computed from the bulk formula following *Fairall et al*. [2003] and *Edson et al*. [2013]:

$$\tau = \rho C_d w^2 \tag{8a}$$

$$\tau_x = \rho C_d w u \tag{8b}$$

$$\tau_y = \rho C_d w v \tag{8c}$$

where ρ is the density of air, C_d drag coefficient. The near-surface air temperature and humidity produced by the OAFlux heat flux project (http://oaflux.whoi.edu) were used in computing the wind profile stability function in Cd.

Given the relationship between τ and w, the uncertainty of τ is related to the uncertainty of w in the following way:

$$\sigma_\tau = \sqrt{\sigma_w^2 \left(\frac{\partial \tau}{\partial w}\right)^2} = \frac{2\tau}{w}\sigma_w \tag{8}$$

Accordingly, the uncertainty of τ_x, denoted σ_{τ_x}, can be derived as follows:

$$\sigma_{\tau_x} = \sqrt{\sigma_u^2 \left(\frac{\partial \tau_x}{\partial u}\right)^2 + \sigma_v^2 \left(\frac{\partial \tau_x}{\partial v}\right)^2 + 2\sigma_{uv}\left(\frac{\partial \tau_x}{\partial u}\right)\left(\frac{\partial \tau_x}{\partial v}\right)} \tag{9}$$

The assumption that the correlation in uncertainties between τ_x and τ_y is negligible simplifies equation (9) to the following form:

$$\sigma_{\tau_x} \approx \sqrt{\sigma_u^2 \left(\tau_x \left(\frac{1}{u} + \frac{u}{w^2}\right)\right)^2 + \sigma_v^2 \left(\tau_x \frac{v}{w^2}\right)^2} \tag{10}$$

Similarly, the uncertainty of τ_y, denoted σ_{τ_y}, can be simplified as

$$\sigma_{\tau_y} \approx \sqrt{\sigma_u^2 \left(\frac{\partial \tau_y}{\partial u}\right)^2 + \sigma_v^2 \left(\frac{\partial \tau_y}{\partial v}\right)^2} = \sqrt{\sigma_v^2 \left(\tau_y \left(\frac{1}{v} + \frac{v}{w^2}\right)\right)^2 + \sigma_u^2 \left(\tau_y \frac{u}{w^2}\right)^2} \tag{11}$$

For the special case such as $u = 0$, equation (10) is the same as equation (8) because $w = abs(v)$. Likewise, equation (11) is identical to equation (8) if $v = 0$. The structure of the mean error fields computed from equations (8), (10), and (11) are not discussed in the following sections, as the analysis bears similarity to that of the error fields of *w*, *u*, and *v*. Note that the correlation in uncertainties between τ_x and τ_y could be significant in certain regions on certain time scales. We used this basic assumption merely to gain a first-order estimation for the wind stress components.

3.3. Results

The mean fields and the estimated errors for *w*, *u*, and *v* over the global oceans averaged over 25 full years (1988–2012) were presented (Figures 3a–3f) and zonal averages of these fields were also shown (Figures 3g–3i). The annual-mean pattern of *u* shows three distinct regimes. The regions in the 30–60 degrees north and south latitudes are dominated by prevailing westerly winds with wind speed exceeding 12 ms^{-1}. The broad subtropical oceans are dictated by the trade winds that have moderate wind speeds ($\sim$8 ms^{-1}). The doldrums near the equator are subject to light-wind ($< 5ms^{-1}$) conditions. The annual-mean pattern of *w* reflects the mean pattern of *u*.

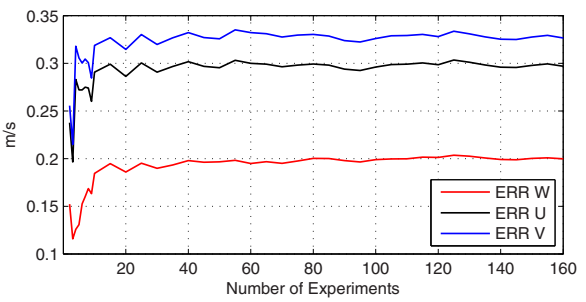

Figure 2. Number of weight perturbation experiments versus the globally averaged STD weight assignment error in wind speed (red line), zonal wind component (black line), and meridional wind component (blue line) for year 2008.

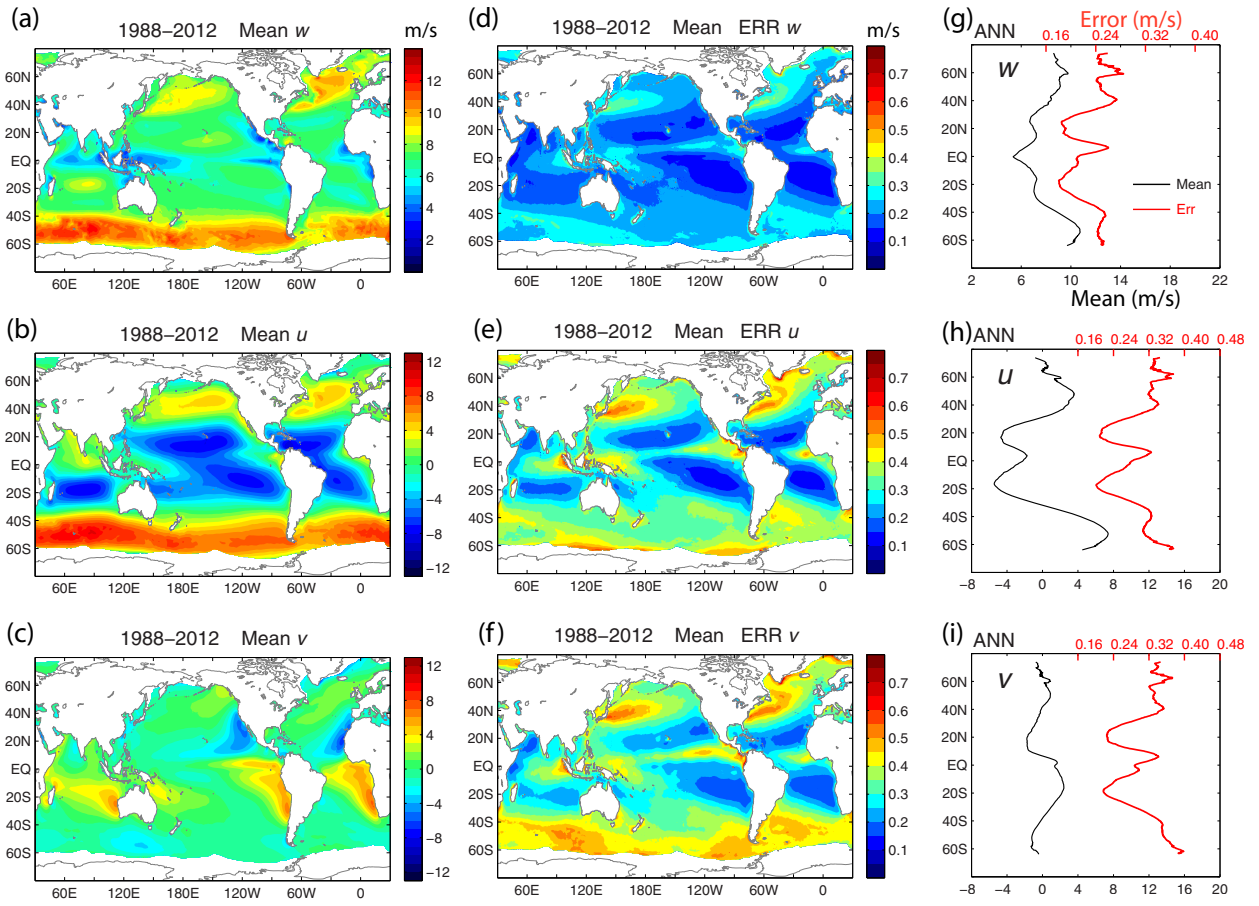

Figure 3. The 25 year time-mean of the OAFlux wind fields and uncertainty estimates in response to the uncertainty in weight assignment. (left) The annual mean fields of (a) wind speed, (b) zonal (positive eastward), and (c) meridional (positive northward) winds. (middle) The annual mean error fields of (d) wind speed, (e) zonal and (f) meridional winds. (right) Zonally averaged annual-mean values for (g) wind speed and associated error estimate, (h) zonal wind and associated error estimate, and (i) meridional wind and associated error estimate.

On the other hand, the annual-mean pattern of *v* shows that the meridional winds associated with the Hadley circulation are the most dominant feature over the global scale. Larger amplitude of the northerlies and southerlies are all located in regions adjacent to the eastern boundary of the basin.

Despite the pattern differences in the annual-mean fields between *u* (or *w*) and *v*, the mean error patterns are surprisingly similar between the three variables, with the largest errors appearing in the same three distinct regions: the westerly belts in the northern and southern midlatitudes (40–60°) and the Intertropical Convergence Zone (ITCZ)/South Pacific Convergence Zone (SPCZ) near the equator. Errors are small in the tropical/subtropical trade-wind regime. The only major difference between the three sets of mean error fields is the magnitude: the errors in *u* and *v* are evidently larger than the error in *w*. When averaged globally and over the 25 year period, the errors induced by the weight-assignment errors are estimated to be 0.21 ms^{-1} in *w*, 0.30 ms^{-1} in *u*, and 0.32 ms^{-1} in *v*.

The 25 year averaged monthly fields in January and July were constructed (Figures 4 and 5) to further delineate the pattern relationship between the mean and error fields. Seasonal changes in *w* and *u* are characterized by the strengthening of the northern (southern) hemispheric westerlies in January (July), while seasonal changes in *v* are featured by an equatorward enhancement of the southeast trades in July. The magnitude of the mean errors increases in accordance with the seasonal enhancement of prevailing winds during the winter season. For instance, large errors are located between 30–60°N in January when the Northern Hemispheric westerlies are seasonally strong, while in July the large errors are located between 30–60°S when the Southern Hemispheric westerlies are seasonally strong. The errors in the ITCZ region, particularly in the eastern tropical Pacific, also become more dominant in July. The zonally averaged plots

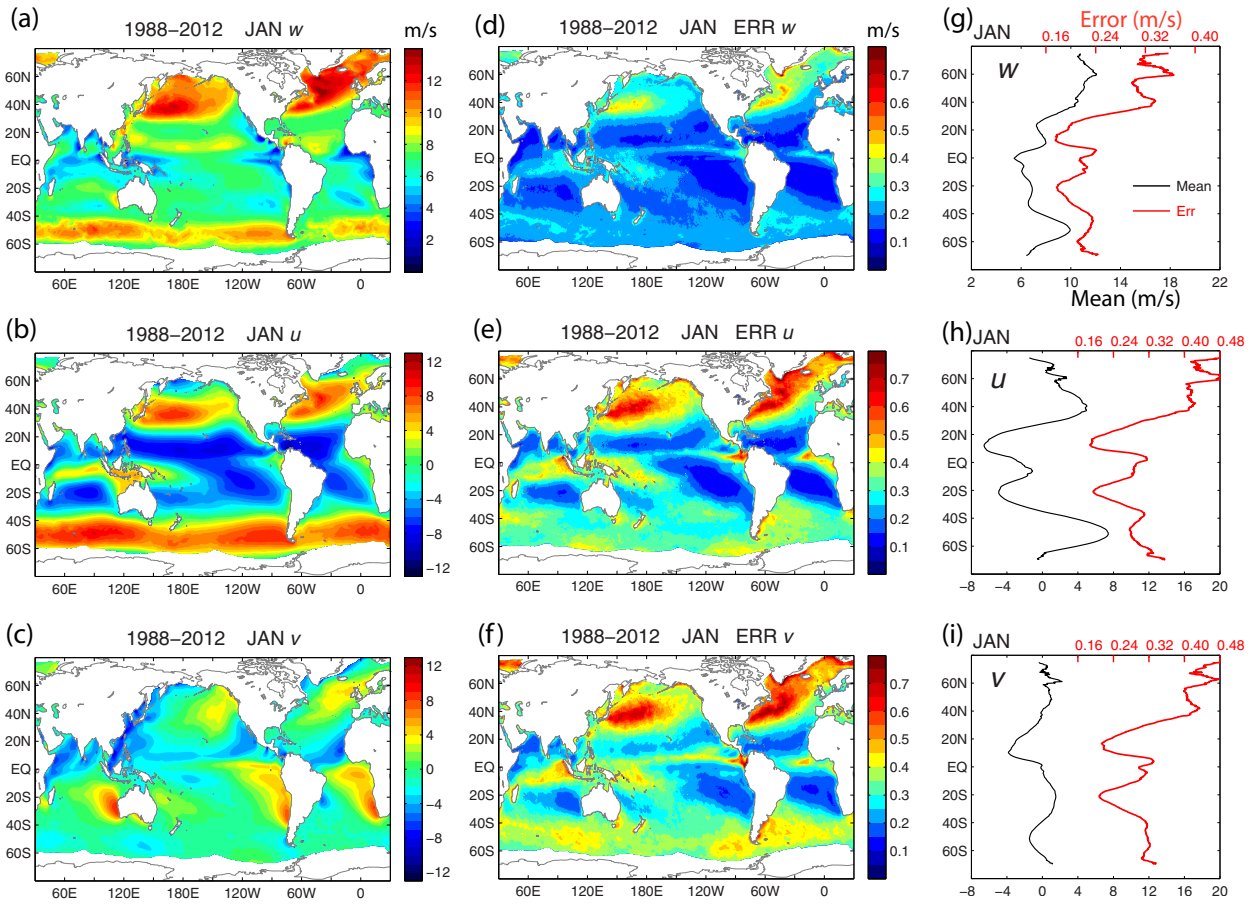

Figure 4. Same as Figure 3 but for time-mean January.

(Figures 4 and 5) provide a good summary of the dependence of errors on the magnitude of wind speed and components. One interesting revelation in these plots is that the errors of the three variables all have a similar latitudinal distribution despite the slight difference in the magnitude.

3.4. Impacts of Rain and High Winds on Error Estimates

The similarity in error spatial structures between *w, u*, and *v* suggests that the errors are not controlled by the magnitude of wind speed and components. As discussed in YJ14, major uncertainty in the daily-mean satellite surface wind retrievals is associated with rain and high winds. The impacts of the two conditions on the uncertainty analysis are investigated here.

The rain flags from the SSM/I series (SSM/I F13, 16, and 17) were counted on a daily basis to form a time series of daily rain mask over the 25 year (1988–2012) period, from which the number of rain days per month was constructed. The time-mean averages for annual mean, January, and July were shown in Figures 6a–6c. Frequent rain days are located in three major latitudinal bands: the ITCZ, the north mid latitudes (30–65°N), and the south mid latitudes (40–65°S), where the latter two are known to be the regions of the mid latitude storm tracks [*Hoskins and Valdes*, 1990]. On average, rain frequency is highest is in the ITCZ/SPCZ regions, with a mean of ~ 16 days per month over most of the Pacific sector. Seasonal changes in the rain frequency are noted. There are more rain days during the boreal summer and less in the boreal winter. The rain frequency associated with the midlatitudes storm tracks also changes with seasons, with enhanced activity during the hemisphere's summer season. However, there is one exception. The North Atlantic features more rain days in January than in July, particularly along the Gulf Stream and its extension.

The number of high winds ($>15 ms^{-1}$) days was also counted using the same SSM/I series (F13, 16, and 17). The 25 year time-mean averages for annual mean, January, and July were shown in Figures 7a–7c. It is

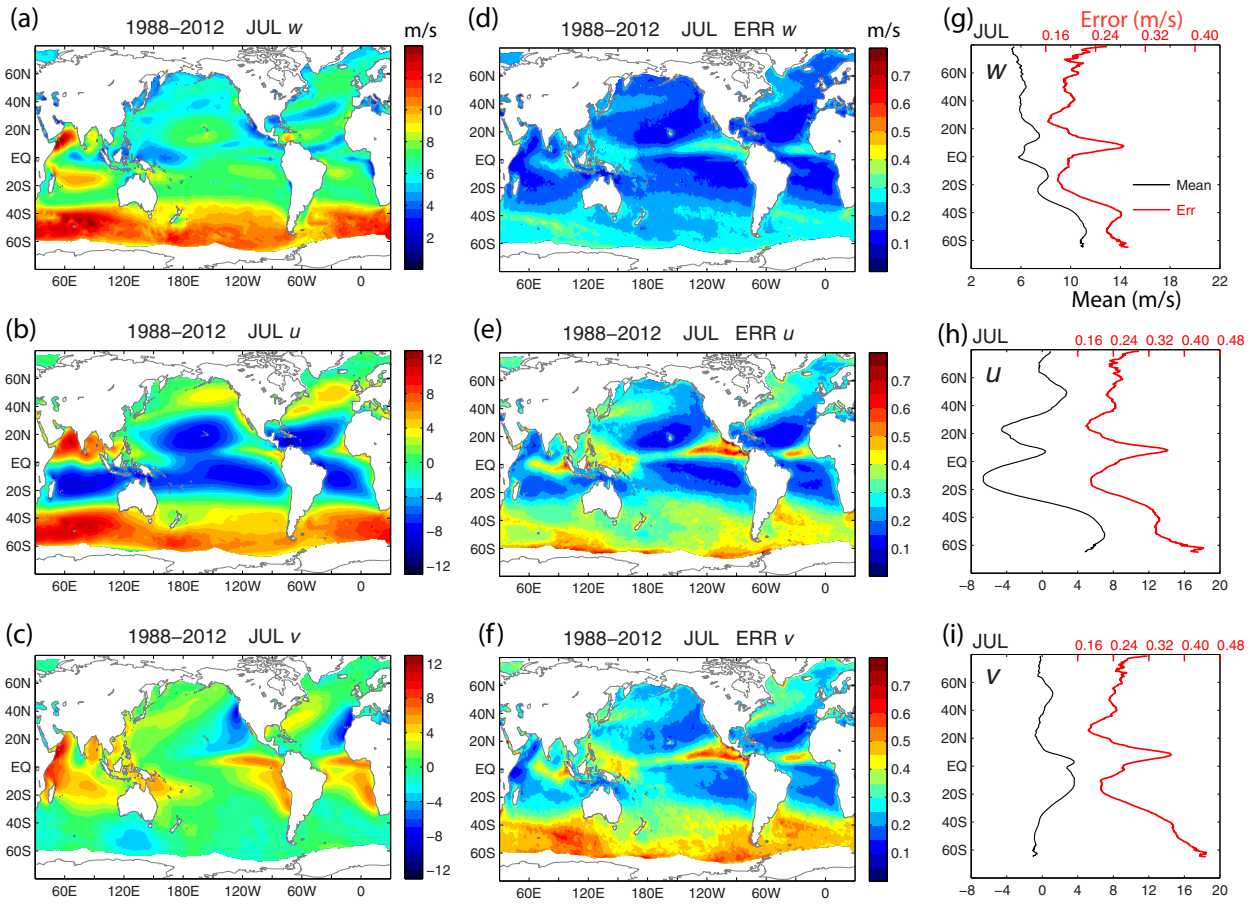

Figure 5. Same as Figure 3 but for time-mean July.

evidenced that high wind events occur predominantly at higher latitudes (poleward 40° north and south) during the hemisphere's winter season. The occurrence of high winds is less frequent than the occurrence of rain, which is averaged about than 10 days per month during the winter season.

Seasonal variations of the rain frequency and high-wind frequency are further summarized in the plots of the zonal averages (Figures 8a and 8b). To examine their respective connection to the estimated error structures in wind speed and components, the plots of the zonally averaged errors of *w, u*, and *v* are included (Figures 8c–8e). One feature stands out in particular: in the tropical oceans where winds are relatively weak, the errors in wind estimates correlate primarily with the rain frequency. On the other hand, in the extratropical regions where winds are subject to strong influence of midlatitude storms, rain, and high wind conditions are equal contributors to the errors in wind estimates. Take the North Atlantic as an example. The frequent rain days and high-wind days in January (Figures 6b and 7b) are associated with large errors in all wind components. High winds are usually correlated with rain in events of severe weather storms. Rain affects microwave sensors with various degrees, as the effect is dependent on the frequency [*Meissner and Wentz*, 2009; *Portabella and Stoffelen*, 2001; *Portabella et al*., 2012; *Stiles and Yueh*, 2002; *Weissman et al*., 2002, 2012]. Microwave radiometers are highly sensitive to rain and thus provide no retrievals in rain conditions. QuikSCAT is sensitive only to heavy rain (i.e., vertically integrated rain rate greater than 2.0 km mm hr^{-1}), while ASCAT is not directly affected by rain. The removal of rain contaminated wind retrievals in QuikSCAT leads to data voids. Reanalyzed winds are the default background fields, but the differences between models and satellites under extreme conditions often do not help to alleviate the problem. In addition, winter storms do not last a full day since they are transient, therefore measurements at different times of day by different satellites are likely to be inconsistent and contribute to the uncertainty in daily mean winds.

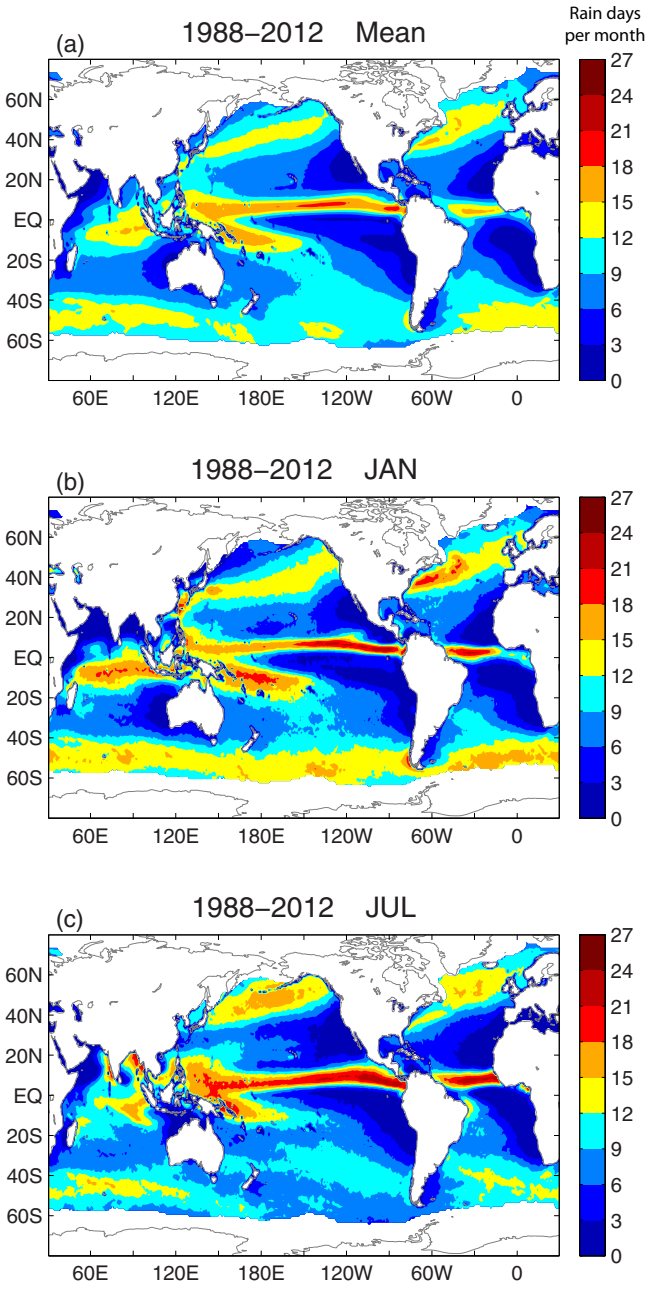

Figure 6. Averaged number of rain days per month constructed from SSM/I and SSMIS sensors (F13, F16, and F17) during the 1988–2012 period. (a) Annual mean, (b) January, and (c) July. Unit: number of days per month.

3.5. Why Are Errors of *u* and *v* Larger Than Errors of *w*?

To understand the cause of the magnitude difference between the errors in *w* and those in *u* and *v*, the impact of high-wind and rain conditions, on the daily wind fields was examined. Here the analysis made on 1 January 2005 is shown (Figures 9 and 10). The rain rate retrievals were derived from SSM/I F13 (Figure 9a), in which narrow bands of rain are evidenced in the tropical regions associated with the ITCZ and SPCZ and also in midlatitudes associated with synoptic weather storms. The daily averaged near-surface wind speed fields from SSM/I F13 (Figure 9b) and QuikSCAT (Figure 9c) show that winds are weaker ($<8\,ms^{-1}$) in the tropics but are highly variable in the extratropical oceans. Bands of strong winds ($>15\ ms^{-1}$) can appear either in the neighborhood of rain bands (e.g., the North Pacific) or with no rain in sight (e.g., the North Atlantic). It is clear that the SSM/I wind speed field has more missing values than the QuikSCAT field, due to the greater sensitivity to rain as well as the larger gaps between swaths.

Seven sensors (SSM/I F13, F14, F15, F16, AMSRE, WindSat wind speed, and QuikSCAT) were included in the synthesis on 1 January 2005. The resulting synthesized fields of *w*, *u*, and *v* (Figures 10a–10c) and the corresponding error estimates (Figures 10d–10f) suggest a close connection between the rain bands and the locations of major errors. For instance, the daily-mean wind fields show that higher winds are organized primarily around the storm's cyclonic circulations in the extratropical oceans, but the exact location of large *u* differs from that of large *v*. The three error fields are found, however, to have a very similar error pattern that resembles the rain pattern (Figure 9a) not the corresponding daily-mean wind field. Take the North Pacific as an example. Four meridional bands of large errors of *v* lie across the area between 120°E and 140°W, each of which is about 20° long. The error bands on the outer sides are associated with the local rain bands, while the middle one along the 180 meridian is in a rain-free area. Interestingly, we found that the contributor to this rain-free error band is the strong northerly winds (Figure 10c). In the cost function (1), the input data sets used for constructing *u* and *v* included QuikSCAT and reanalyses from ERAinterim and CFSR, while the input data sets used for *w* had satellite retrievals from seven sensors. Thus, the reanalyzed fields have different roles in producing an estimate for (*u*, *v*) and *w*. The

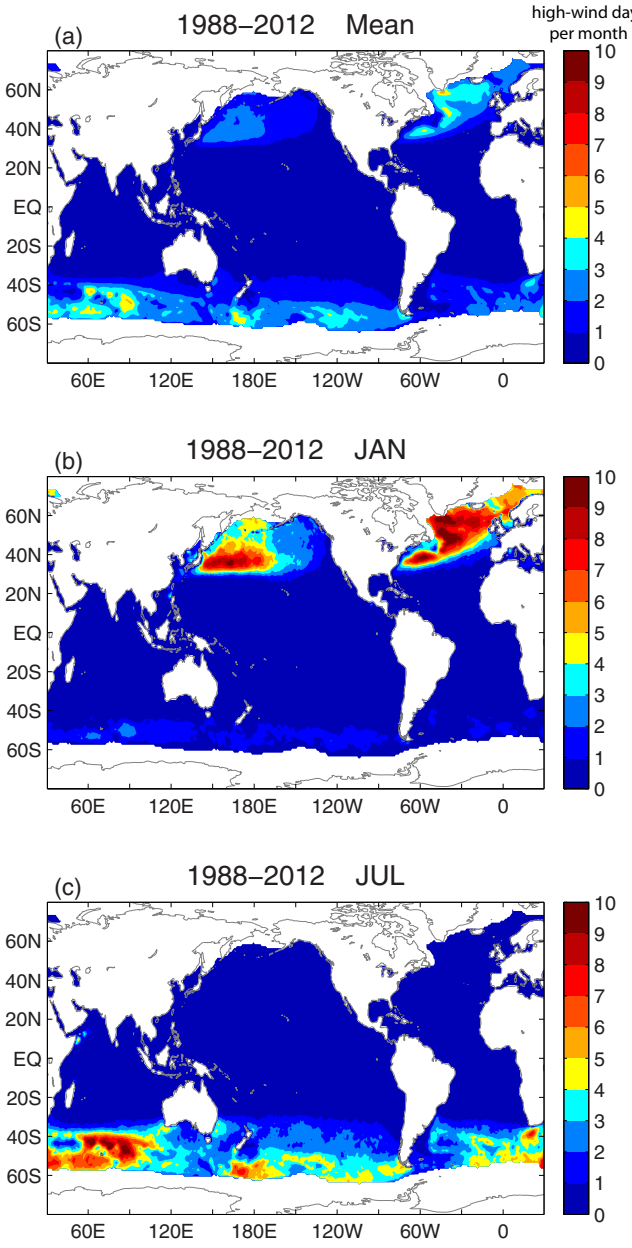

Figure 7. Averaged number of high-wind (>15 ms^{-1}) days per month constructed from SSM/I and SSMIS sensors (F13, F16, and F17) during the 1988–2012 period. (a) Annual mean, (b) January, and (c) July. Unit: number of days per month.

reanalyzed *w* fields were not used as a data constraint but the reanalyzed *u* and *v* fields were part of data constraints (e.g., term (I) in cost function (1)). Despite that the weight assignments for the reanalyses were much weaker than those for the satellites (i.e., the ratio between the total reanalysis constrains and the total satellite constraints is 1.2:11; see Figure 1), the reanalyses, by default, have a larger influence on the estimation of *u* and *v* than on the estimation of *w*. In events of weather storms, the reanalyzed winds are generally weaker than the satellite winds, and the differences are not easy to reconcile [see YJ14] and translate into an uncertainty of the *u* and *v* estimates.

3.6. Rain and High Winds Detected by SSM/I and QuikSCAT

The wind speed retrievals from the SSM/I series are derived from the measurements made at 37 GHz channels, while the wind speed and vector retrievals from QuikSCAT are made at 14 GHz. Higher frequency bands are more sensitive to rain than lower frequency bands. As a result, SSM/I provides no wind retrievals whenever there is rain, whereas QuikSCAT is only sensitive to heavy rain (i.e., rain rate greater than 15 mm hr^{-1}). It is, therefore, expected that SSM/I has more rain-flagged days than QuikSCAT or equivalently, less useful wind retrievals from one SSM/I sensor than from QuikSCAT on a daily basis.

The QuikSCAT product used in this study was the version 4 product from the Ku-2011 GMF by the Remote Sensing Systems (RSS) [*Ricciardulli and Wentz*, 2011]. The product has two sets of rain flag. One set was derived directly from the scatterometer and the other based on the collocated radiometer columnar rain rates from SSM/Is (F13, F14, and F15) and TMI. Both rain flags were applied in identifying rain-contaminated wind vector cells. The wind vector cell was removed whenever one rain flag showed a rain.

The total rain amount derived from SSM/I F13 (Figure 11a) is shown to help elucidate the difference between the total number of rain days derived from the SSM/I F13 and that derived from QuikSCAT (Figures 11b and 11c). Daily-mean fields in 2008 are used here for characterization. The difference is most apparent in the three rain bands: the tropical ITCZ/SPCZ, and the extratropical storm tracks at the northern and southern midlatitudes (40–60°). The SSM/I wind retrievals register more than 180 rain-flagged days for the areas that have the total SSMI rain amount greater than 120 cm over the year (Figures11a and 11b). By

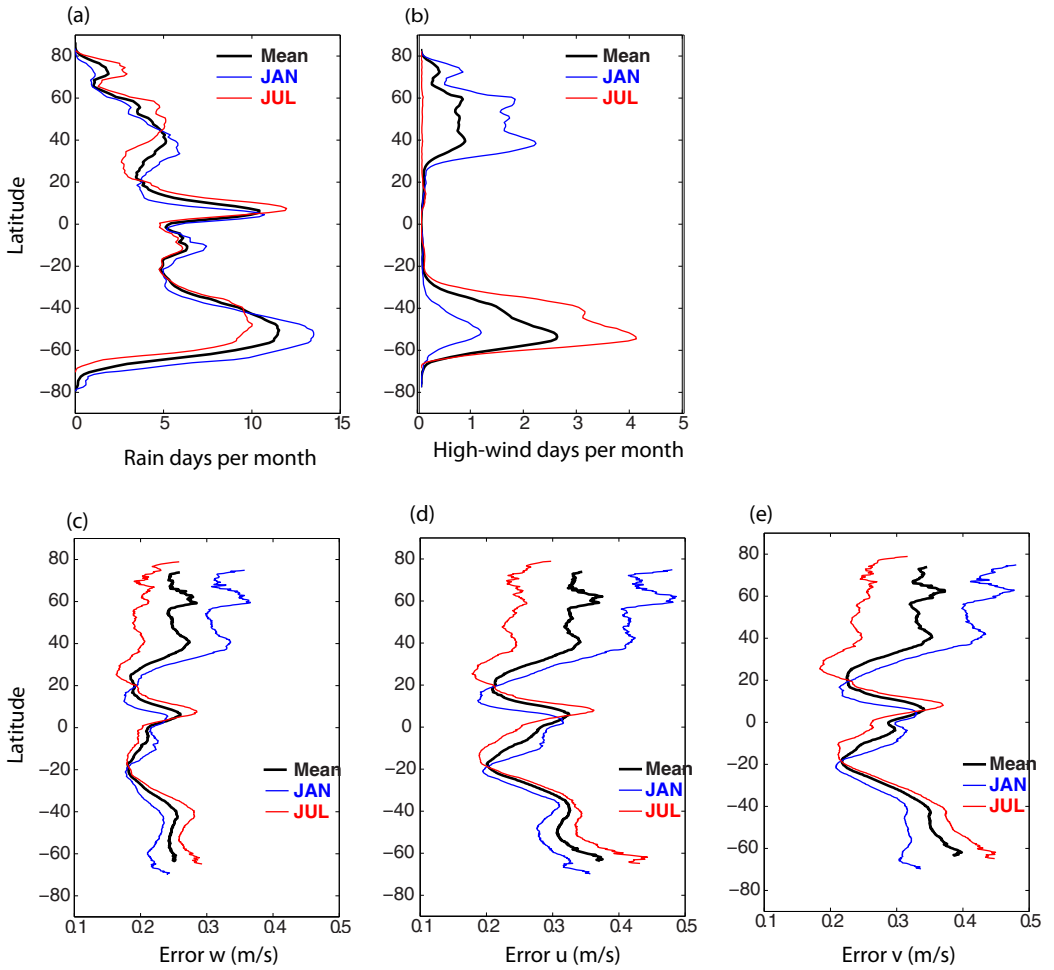

Figure 8. Zonally averaged values for annual mean (thick black), January (blue), and July (red) over the 25 year period (1988–2012). (a) Rain days per month, (b) High wind days per month, (c) estimated error of wind speed, (d) estimated error of zonal wind, and (e) estimated error of meridional wind.

comparison, the QuikSCAT wind retrievals show that the rain-flagged days of greater than 180 occur in much smaller areas, associated mostly with the annual rain amount exceeding 240 cm (Figures 11a and 11c). The advantage of QuikSCAT over SSM/I in providing more valid retrievals under similar rain conditions is evident.

To check the consistency in the high-wind retrievals between the two types of sensors, the number of high-wind days derived from SSM/I is compared with that derived from QuikSCAT for the year 2008 (Figures 12a–12c). The two sensors produce a very similar pattern with also a similar frequency range (Figures 12a and 12b). The correlation of the two high-wind patterns is 0.95, which is significant at the 95% confidence level. SSM/I has slightly more high-wind days at a few spots, such as the north Atlantic near 50°N and the southern Indian Ocean near 45°S. The northern Atlantic Ocean had about 50–60 days of high winds in 2008, while the northern Pacific had about 20–30 days on average. In the southern oceans, high winds are embedded within the strong westerly wind belt and are most frequent in the Indian and Pacific sectors with an average of 50–60 days per year. The high-wind frequency derived from SSMIS, ASMRE, and WindSat (not shown) is similar to that from SSM/I, due mostly to the use of the same RTM in retrieving winds from these sensors.

3.7. Dependence of the Estimated Errors on Rain Intensity and Wind Speed

The discussions above delineated that the ensemble error statistics of *w*, *u*, and *v* generated by the weight perturbation analysis are capable of identifying the impact of rain and high wind conditions on the OAFlux analysis. To characterize the dependence of the estimated errors of *w*, *u*, and *v* on rain intensity and wind speed in their full ranges, the errors were binned onto the SSM/I rain rate bin of every 50 cm yr^{-1} and the

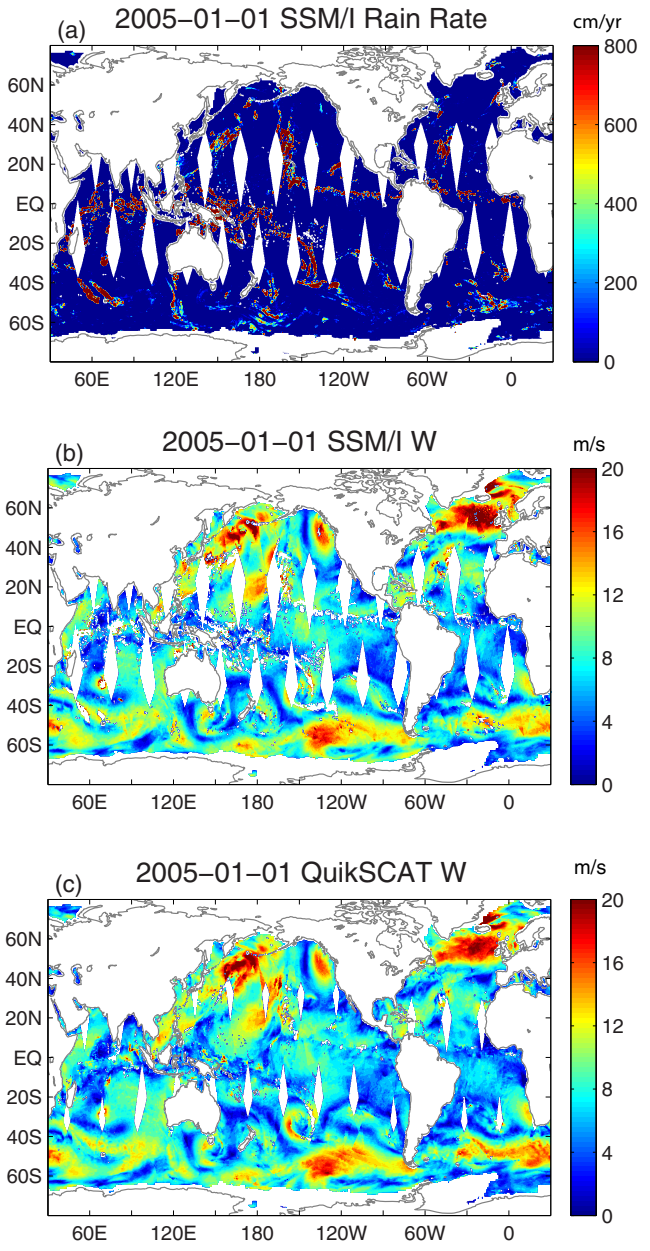

Figure 9. Case study of daily-mean fields from satellite observations on 1 January 2005. (a) Rain rate from SSM/I F13, (b) wind speed from SSM/I F13, and (c) wind speed from QuikSCAT.

SSM/I wind speed bin of every 1 ms^{-1} (Figures 13a and 13b). It can be seen that the magnitude of the errors of *w*, *u*, and *v* increases gradually with rain intensity. For the rain rate in the range of 0–1000 cm yr^{-1}, the *w* errors increase from 0.2 to 0.3 ms^{-1} and the *u* and *v* errors from 0.3 to 0.6 ms^{-1}. As discussed in section 3.5, the greater sensitivity of *u* and *v* errors to rain intensity (Figure 10) underlines the complication of using the reanalysis winds to fill in the rain-induced data voids in QuikSCAT. On the other hand, the reduced sensitivity of the *w* errors to rain intensity reflects the fact that there are more radiometers than scatterometers and the nearly 100% wind speed coverage on a daily basis requires little or no usage of the background reanalysis fields.

The association of the *w*, *u*, and *v* errors with the wind speed (Figure 13b) depicts a striking influence of high winds. At low to moderate wind speed range (2–10 ms^{-1}), the errors of *w*, *u*, and *v* remain leveled at around 0.2 ms^{-1} for *w* and 0.3 ms^{-1} for *u* and *v*. Once the wind speed exceeds 10 ms^{-1}, all errors start to increase sharply. In particular, when the wind speed strengthens from 15 to 20 ms^{-1}, errors of *u* and *v* is up from 0.4 to 0.6 ms^{-1} and errors of *w* from 0.2 to 0.4 ms^{-1}. Errors of *v* appear to be more sensitive to high wind conditions and has the largest rate of increase with wind speed.

4. Summary and Discussion

A high-resolution global analysis of ocean-surface vector winds from 1987 onward has been recently developed by the OAFlux project through objective synthesis of 12 satellite wind sensors [*Yu and Jin* 2014]. The 12 satellite sensors include 2 scatterometers (QuikSCAT and ASCAT) that have wind speed and direction retrievals, and 10 passive microwave radiometers (six SSM/I sensors—F08, F10, F11, F13, F14, and F15; two SSMIS sensors—F16 and F17, AMSR-E, and the passive polarimetric microwave radiometer from WindSat) that have wind speed retrievals only. A variational approach was used to find a best fit to input data (satellite observations, reanalysis wind components, and a priori terms) in a weighted least-squares cost function. Since the weights are inversely proportional to error covariances of data and error covariances cannot be perfectly known, the best-fit of the cost function is sensitive to the uncertainty of the weight assignments.

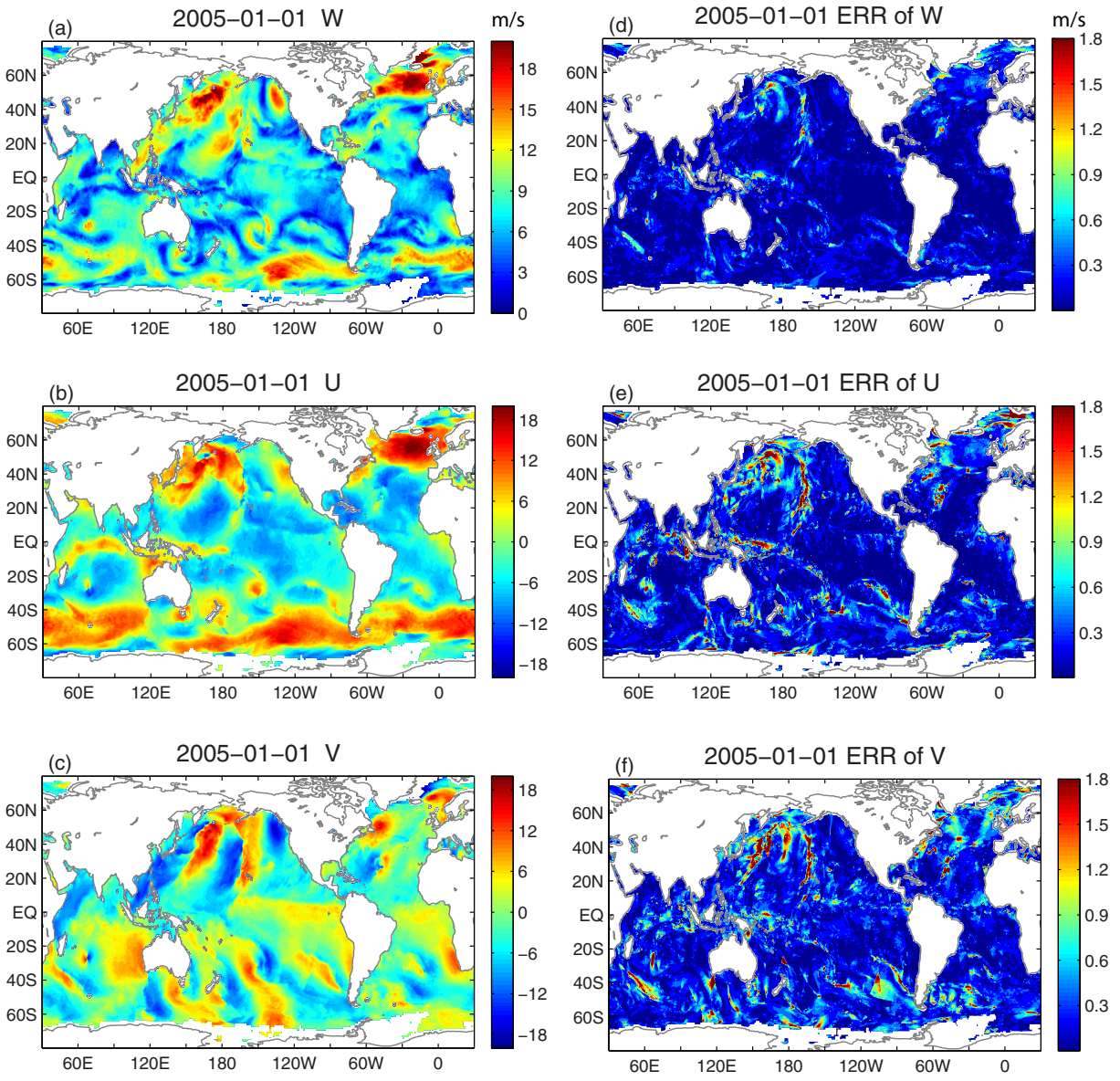

Figure 10. Case study of the OAFlux daily-mean winds and associated error estimates on 1 January 2005. (a) Wind speed, (b) zonal wind, (c) meridional wind, (d) estimated error of wind speed, (e) estimated error of zonal wind, and (f) estimated error of meridional wind.

This study aims to providing confidence and sensitivity analysis to the newly developed OAFlux vector wind time series and to complementing the study of *Yu and Jin* [2014]. Two issues are addressed. The first issue is the selection of the optimal weights used for the OAFlux synthesis. A set of weight-varying experiments was conducted, from which the weights were selected by satisfying the condition that the chosen weights should make the best-fit of the cost function be optimal with regard to both input satellite observations and the air-sea buoy measurements at 126 locations (Figure 1). The buoy measurements were not part of the synthesis and served as an independent measure in the selection.

The idea of the weight selection experiments was inspired by the study of *Desroziers and Ivanov* [2001] in that the error covariance parameters can be tuned adaptively using the diagnostics of the differences between the solution of the cost function and input observations (i.e., the innovation vectors). We demonstrated in our study that independent buoy measurements are an effective addition in selecting the optimal weights needed in the cost function. A total of 200 experiments

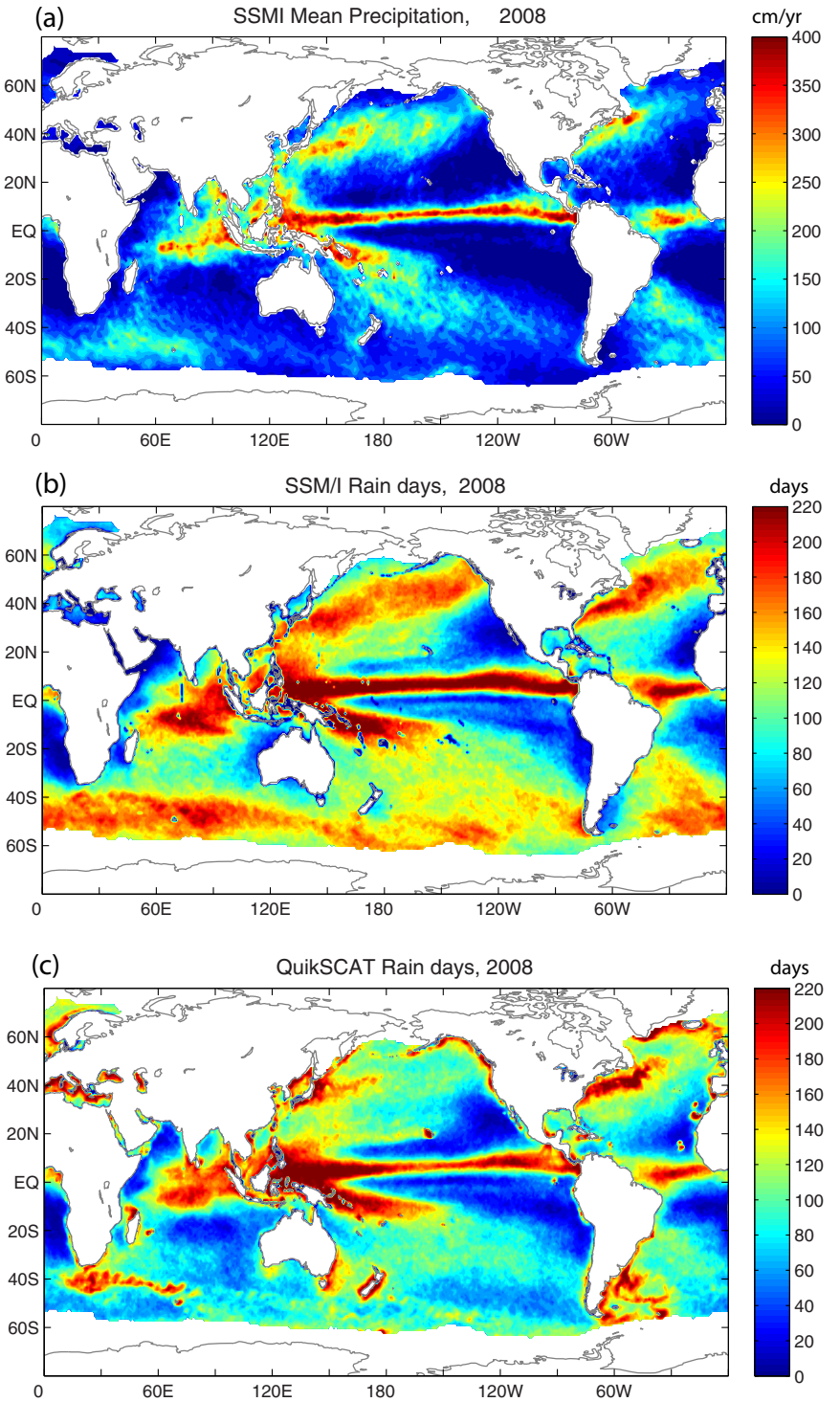

Figure 11. (a) Annual-mean averaged rain rate in 2008 derived from SSM/I F13, (b) the total number of rain days in 2008 constructed from SSM/I F13, and (c) the total number of rain days in 2008 from QuikSCAT.

were conducted to test the performance of the cost function in response to various weight ratios between the total weights assigned to satellite data constraints and those to reanalyses constraints, from which an optimal ratio was determined. However, details of the spatial structure and temporal variability of the errors cannot be deduced due to the limited coverage of the buoy measurements. The experiment was limited to the weights that were assumed to be constant and

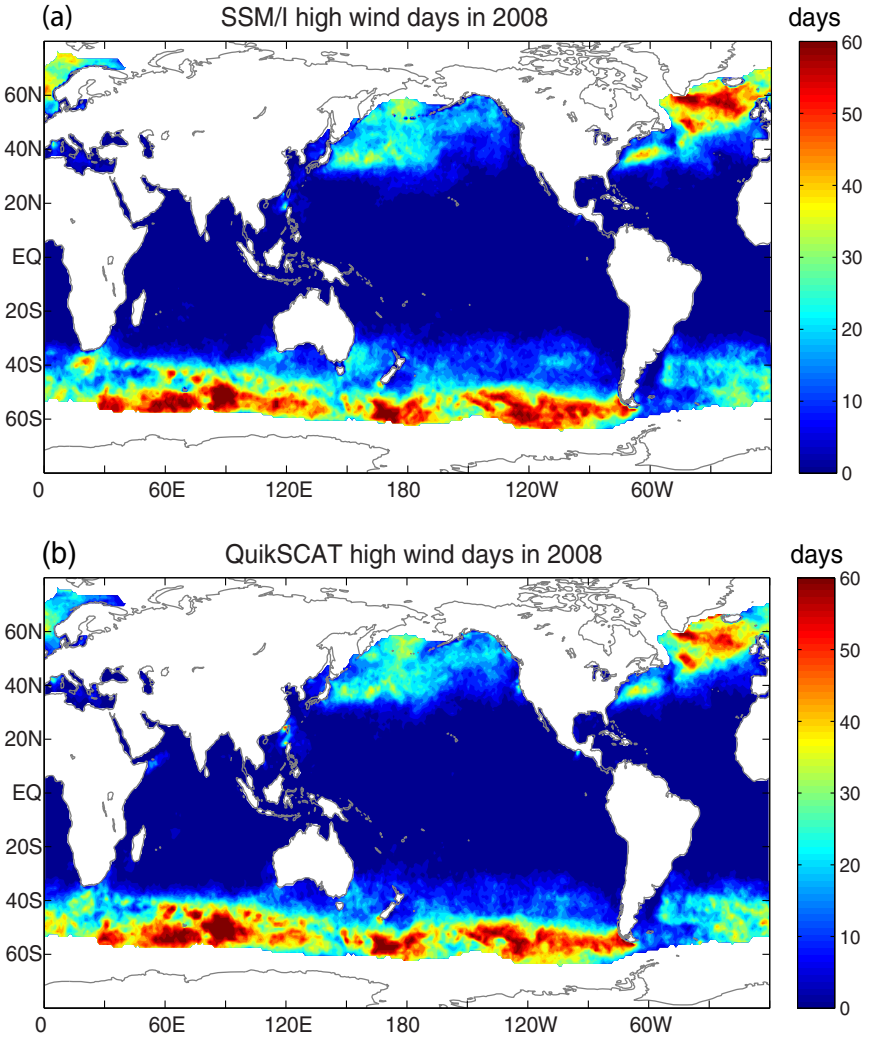

Figure 12. The total number of high-wind days in 2008 constructed from (a) SSM/I F13 and (b) QuikSCAT.

the selection criteria was based on the gross impact of the weights on the minimization of the cost function.

Determining the uncertainty of the wind analysis associated with the uncertainty in the weight assignments in both spatial and temporal domain is the second issue addressed in the study. This was achieved by designing ensemble-based weight perturbation experiments to generate an ensemble of the solutions in response to randomized weights and to use the ensemble statistics as a measure of the uncertainty of the solution due to the uncertainty of the weight assignments. A total of 160 sets of weight perturbation experiments were conducted (Figure 2). The ensemble statistics approach a quasi steady state when N is around 40, and the further increase of the number of experiments does not change the statistics as the degree of freedom for errors is determined by the number of input data sets not by the number of sensitivity experiments. The ensemble statistics led to the characterization of the effect of the weight assignment errors on the vector wind analysis (Figures 3–5). When averaged globally and over the 25 year analysis period, the estimated mean STD weight assignment error is 0.21 ms^{-1} in w, 0.30 ms^{-1} in u, and 0.32 ms^{-1} in v.

High winds ($>15ms^{-1}$) and rain conditions are identified as the leading sources of uncertainty in the OAFlux wind analysis (Figure 13). The three error fields of w, u, and v are shown to have a similar spatial pattern, with large errors appearing in three distinct regions: the westerly belts in the northern and southern

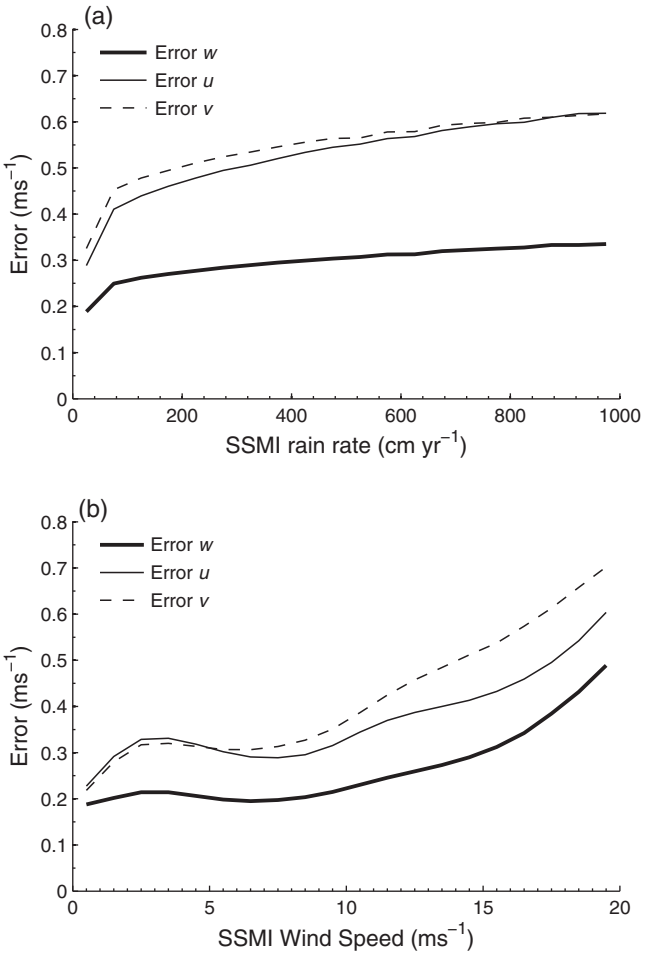

Figure 13. Increase of the wind speed error with (a) SSM/I F13 rain rate and (b) SSM/I F13 wind speed constructed from daily-mean fields in 2008.

midlatitudes (40–60°) and the ITCZ/SPCZ rain belts in the tropical oceans (Figures 6–8). It is evidenced that the error patterns are not controlled by the magnitude of wind speed and components but by the patterns of high winds and rain rate. Wind retrievals from different sensors differ at high wind speeds due to the lack of the ground-based high-wind measurements as validation (Figure 12). The effect of rain on microwave sensors depends on the operating frequency, with QuikSCAT retrievals being contaminated under heavy rain (Figure 11). It is found that the removal of rain contaminated wind retrievals in QuikSCAT leads to data voids in *u* and *v* components which cannot be filled in directly by reanalysis winds. The differences between satellite and reanalysis wind fields are usually large in events of synoptic storms, which are the source of uncertainty in weight assignments as well as in the wind analysis (Figures 9 and 10). Winter storms do not last a full day since they are transient, therefore measurements at different times of day by different satellites are likely to be inconsistent and contribute to the uncertainty in daily mean winds. On the other hand, the errors of *w* are less affected by the inclusion of reanalysis, because there are more radiometers than scatterometers and the nearly 100% wind speed coverage on a daily basis requires little or no usage of the background reanalysis fields. Apparently, the need of reanalysis winds is due predominantly to the need of filling in data voids in vector wind components not in the wind speed.

Given the complexity of the sources contributing to errors, the present analysis of errors represents the first effort we made toward improving the characterization and quantification of the uncertainty in the OAFlux vector wind analysis associated with the weight assignment errors. High winds correlated with rain remain a major technical challenge for proper wind retrievals from satellites. The multisensor synthesis is not expected to mitigate the impacts of missing retrievals in events of severe weather. It becomes apparent that further improvement of the multisensor synthesis in events of severe storms will rely on the future technical advancement in retrieval algorithms to better apprehend and comprehend the wind retrievals under extreme weather conditions. Recently, the satellite ocean-wind observing system reaches a historical three-scatterometer constellation that features ASCAT aboard EUMESAT MetOP-A and -B, and the Indian OceanSat-2 scatterometer (OSCAT) launched by ISRO. ASCAT-A and ASCAT-B are less sensitive to rain and OSCAT has a global daily coverage equivalent to QuikSCAT. However, the demise of OSCAT in February 2014 let the way for the Chinese HaiYang (HY)—2A scatterometer to be an important replacement once data are made available to the wind research community. The three scatterometers when combined present an exciting opportunity to improve the understanding and estimation of the wind estimates under all weather conditions and to continue the satellite vector wind time series beyond QuikSCAT.

Acknowledgments
The project is sponsored by the NASA Ocean Vector Wind Science Team (OVWST) activities under grant NNA10AO86G. The database of 126 buoys was established during the development of the OAFlux surface turbulent latent and sensible heat fluxes under the auspices of the NOAA grant NA09OAR4320129. The satellite wind products of SSMI, SSMIS AMSRE, and QuikSCAT were downloaded from Remote Sensing Systems at http://www.ssmi.com/, and ASCAT data sets from NASA JPL PO.DAAC at http://podaac.jpl.nasa.gov. The original ASCAT data sets are hosted by KNMI at http://www.knmi.nl/scatterometer. The ERA-interim winds were from NCAR Research Data Archive at http://dss.ucar.edu and the original data sets are produced by ECMWF. CFSR winds were obtained from NCEP/CFSR data archives at NCDC NOMADS data access.

References

ASCAT Wind Product User Manual (2013), *ASCAT Wind Product User Manual*, version 1.13, Ocean and Sea Ice SAF, 23 pp., The Royal Netherlands Meteorological Institute (KNMI), Utretht, Netherlands. [Available at http://www.knmi.nl/scatterometer/publications/pdf/ASCAT_Product_Manual.pdf.]

Atlas, R., R. N. Hoffman, J. Ardizzone, S. M. Leidner, J. C. Jusem, D. K. Smith, and D. Gombos (2011). A cross-calibrated, multiplatform ocean surface wind velocity product for meteorological and oceanographic applications, *Bull. Am. Meteorol. Soc.*, *92*, 157–174, doi:10.1175/2010BAMS2946.1.

Bannister R. N. (2007), Can wavelets improve the representation of forecast error covariances in variational data assimilation?, *Mon. Weather Rev.*, *135*, 387–408.

Berre, L., S. Stefanescu, and M. Belo Pereira, (2006), The representation of analysis effect in three error simulation techniques. *Tellus Ser A*, *58*, 196–209.

Bentamy, A., S. A. Grodsky, J. A. Carton, D. Croizé-Fillon, and B. Chapron, (2012), Matching ASCAT and QuikSCAT winds, *J. Geophys. Res.*, *117*, C02011, doi:10.1029/2011JC007479.

Bonavita, M, L. Isaksen, and E. Hólm (2012), On the use of EDA background error variances in the ECMWF 4D-Var, *Q. J. R. Meteorol. Soc.*, *138*, 1540–1559, doi:10.1002/qj.1899.

Bourassa, M. A., and K. M. Ford, (2010), Uncertainty in scatterometer-derived vorticity, *J. Atmos. Oceanic Technol.*, *27*, 594–603, doi:10.1175/2009JTECHO689.1.

Bourassa, M. A., D. M. Legler, J. J. O'Brien, and S. R. Smith (2003), SeaWinds validation with research vessels, *J. Geophys. Res.*, *108*, C2, 3019.

Buehner, M., P. Gauthier, and Z. Liu (2005), Evaluation of new estimates of background- and observation-error covariances for variational assimilation. *Q. J. R. Meteorol. Soc.*, *131*, 3373–3383.

Chapnik, B., G. Desroziers, F. Rabier, and O. Talagrand (2004), Properties and first application of an error statistics tuning method in a variational assimilation. *Q. J. R. Meteorol. Soc.*, *130*, 2253–2275.

Courtier, P., J.-N. Thepaut, and A. Hollingsworth (1994), A strategy for operational implementation of 4D-Var using an incremental approach, *Q. J. R. Meteorol. Soc.*, *120*, 1367–1387.

Courtier, P., E. Andersson, W. Heckley, J. Pailleux, D. Vasiljevic, M. Hamrud, A. Hollingsworth, F. Rabier, M. Fisher, and J. Pailleux (1998), The ECMWF implementation of three-dimensional variational assimilation (3D-VAR). Part I: Formulation. *Q. J. R. Meteorol. Soc.*, *124*, 1783–1807.

Daley, R. (1991), *Atmospheric Data Analysis*, 457 pp., Cambridge Univ. Press, Cambridge, U. K.

Dee, D. P. (2005), Bias and data assimilation, *Q. J. R. Meteorol. Soc.*, *131*, 3323–3343.

Dee, D. P., et al. (2011), The ERA-Interim reanalysis: Configuration and performance of the data assimilation system, *Q. J. R. Meteorol. Soc.*, *137*, 553–597, doi:10.1002/qj.828.

Desroziers, G., and S. Ivanov (2001), Diagnosis and adaptive tuning of information-error parameters in a variational assimilation, *Q. J. R. Meteorol. Soc.*, *127*, 1433–1452.

Desroziers, G., L. Berre, B. Chapnik, and P. Poli (2005), Diagnosis of observation, background and analysis-error statistics in observation space, *Q. J. R. Meteorol. Soc.*, *131*, 3385–3396.

Desroziers, G., L. Berre, V. Chabot, and B. Chapnik (2009), A Posteriori diagnostics in an ensemble of perturbed analyses, *Mon. Weather Rev.*, *137*, 3420–3436, doi:10.1175/2009MWR2778.1.

Dunbar, R., et al. (2006), QuikSCAT science data product user manual, version 3.0, *JPL Doc. D-18053—Rev. A*, 85 pp., Jet Propul. Lab., Pasadena, Calif.

Ebuchi, N., H. C. Graber, and M. J. Caruso (2002), Evaluation of wind vectors observed by QuikSCAT/SeaWinds using ocean buoy data, *J. Atmos. Oceanic Technol.*, *19*, 2049–2069.

Edson, J. B., V. Jampana, R. A. Weller, S. Bigorre, A. J. Plueddemann, C. W. Fairall, S. D. Miller, L. Mahrt, D. Vickers, and H. Hersbach (2013), On the exchange of momentum over the open ocean, *J. Phys. Oceanogr.*, *43*, 1589–1610.

Evensen, G. (1994), Sequential data assimilation with a nonlinear quasigeostrophic model using Monte Carlo methods to forecast error statistics, *J. Geophys. Res.*, *99*, 10,143–10,162.

Fairall, C. W., E. F. Bradley, J. E. Hare, A. A. Grachev, and J. B. Edson (2003), Bulk parameterization of air-sea fluxes: Updates and verification for the COARE algorithm, *J. Clim.*, *16*, 571–591.

Fangohr, S., and E. C. Kent (2012), An estimate of structural uncertainty in QuikSCAT wind vector retrievals, *J. Appl. Meteorol. Climatol.*, *51*, 954–961.

Fisher, M. (2003), Background error covariance modelling, Proceedings of the ECMWF Seminar on Recent developments in Data Assimilation for Atmosphere and Ocean, pp. 45–63, Reading, U. K.

Fore, A. G., B. W. Stiles, A. H. Chau, B. A. Williams, R. S. Dunbar, and E. Rodriguez (2014), Point-wise wind retrieval and ambiguity removal improvements for the QuikSCAT climatological data set, *IEEE Trans. Geosci. Remote Sens.*, *52*(1), 51–59, doi:10.1109/TGRS.2012.2235843.

Frehlich, R. (2011), The definition of 'truth' for numerical weather prediction error statistics, *Q. J. R. Meteorol. Soc.*, *137*, 84–98.

Freilich, M. H. (1997), Validation of vector magnitude data sets: Effects of random component errors, *J. Atmos. Oceanic Technol.*, *14*, 695–703.

Harris, B. A., and G. Kelly (2001), A satellite radiance-bias correction scheme for data assimilation, *Q. J. R. Meteorol. Soc.*, *127*, 1453–1468.

Hoffman, R. N. (1984), SASS wind ambiguity removal by direct minimization. Part II: Use of smoothness and dynamical constraints, *Mon. Weather Rev.*, *112*, 1829–1852.

Hoffman, R. N., S. M. Leidner, J. M. Henderson, R. Atlas, J. V. Ardizzone, and S. C. Bloom, (2003), A two-dimensional variational analysis method for NSCAT ambiguity removal: Methodology, sensitivity, and tuning, *J. Atmos. Oceanic Technol.*, *20*, 585–605.

Hoskins, B. J., and P. J. Valdes (1990), On the existence of storm-tracks, *J. Atmos. Sci.*, *47*, 1854–1864. doi:10.1175/1520-0469(1990)047<1854:OTEOST>2.0.CO;2.

Houtekamer, P., L. Lefaivre, J. Derome, H. Ritchie, and H. Mitchell (1996), A system simulation approach to ensemble prediction, *Mon. Weather Rev.*, *124*, 1225–1242.

Kent, E. C., and P. G. Challenor (2006), Toward estimating climatic trends in SST. Part II: Random errors, *J. Atmos. Oceanic Technol.*, *23*(3), 476–486, doi:10.1175/JTECH1844.1.

Kent, E.C., and A. Kaplan (2006), Toward estimating climatic trends in SST. Part III: Systematic biases, *J. Atmos. Oceanic Technol.*, *23*(3), 487–500, doi:10.1175/JTECH1845.1.

Legler, D. M., I. M. Navon, and J. J. O'Brien (1989), Objective Analysis of pseudo-stress over the Indian Ocean using a direct minimization approach, *Mon. Weather Rev.*, *117*, 709–720.

Lorenc, A. C., (1988). Optimal nonlinear objective analysis, *Q. J. R. Meteorol. Soc.*, *114*, 205–240.

Meissner, T., and F. J. Wentz (2009), Wind vector retrievals under rain with passive satellite microwave radiometers, *IEEE Trans. Geosci. Remote Sens.*, *47*(9), 3065–3083.
Milliff, R. F., J. Morzel, D. B. Chelton, and M. H. Freilich, (2004), Wind stress curl and wind stress divergence biases from rain effects on QSCAT surface wind retrievals, *J. Atmos. Oceanic Technol.*, *21*, 1216–1231, doi:10.1175/1520-0426(2004)021<1216:WSCAWS>2.0.CO;2.
Portabella, M., and A. Stoffelen (2001), Rain detection and quality control of sea winds, *J. Atmos. Oceanic Technol.*, *18*(7), 1171–1183.
Portabella, M., A. Stoffelen, W. Lin, A. Turiel, A. Verhoef, J. Verspeek, and J. Ballabrera-Poy (2012), Rain effects on ASCAT-retrieved winds: Toward an improved quality control, *IEEE Trans. Geosci. Remote Sens.*, *50*(7), 2495–2506.
Ricciardulli, L., and F. J. Wentz (2011), Reprocessed QuikSCAT (V04) wind vectors with Ku-2011 geophysical model function, 8 pp., *Rep. 043011*, Remote Sens. Syst., Santa Rosa, Calif.
Sadiki, W., and C. Fischer (2005), A posteriori validation applied to the 3D-VAR Arpege and Aladin data assimilation systems, *Tellus Ser. A*, *57*, 21–34.
Saha, S., et al. (2010), The NCEP climate forecast system reanalysis, *Bull. Am. Meteorol. Soc.*, *91*, 1015–1057, doi:10.1175/2010BAMS3001.1.
Schlax, M. G., D. B. Chelton, and M. H. Freilich (2001), Sampling errors in wind fields constructed from single and tandem scatterometer data sets, *J. Atmos. Oceanic Technol.*, *18*, 1014–1036.
Stiles, B., and S. Yueh (2002), Impact of rain on wind scatterometer data, *IEEE Trans. Geosci. Remote Sens.*, *40*, 1973–1983.
Stoffelen, A. (1998), Toward the true near-surface wind speed: Error modeling and calibration using triple collocation, *J. Geophys. Res.*, *103*, 7755–7766.
Stoffelen, A., and D. Anderson (1997), Scatterometer data interpretation: Estimation and validation of the transfer function CMOD4, *J. Geophys. Res.*, *102*, 5767–5780.
Talagrand, O. (1997), Assimilation of observations, an introduction, *J. Meteorol. Soc. Jpn.*, *75*, 191–209.
Talagrand, O. (1999), A posteriori verification of analysis and assimilation algorithms, in *Proceedings of Workshop on Diagnosis of Data Assimilation Systems*, pp 17–28, 2–4 November 1998, ECMWF, Reading, U. K.
Vogelzang, J., and A. Stoffelen (2012), NWP model error structure functions obtained from scatterometer winds, *IEEE Trans. Geosci. Remote Sens.*, *50*(7), 2525–2533.
Vogelzang, J., A. Stoffelen, A. Verhoef, and J. Figa-Saldaña (2011), On the quality of high-resolution scatterometer winds, *J. Geophys. Res.*, *116*, C10033, doi:10.1029/2010JC006640.
Wahba, G., D. Johnson, F. Gao, and J. Gong (1995), Adaptative tuning of numerical weather prediction models: Randomized GCV in three- and four-dimensional data assimilation, *Mon. Weather Rev.*, *123*, 3358–3369.
Weissman, D., M. A. Bourassa, and J. Tongue (2002), Effects of rain rate and magnitude on SeaWinds scatterometer wind speed errors, *J. Atmos. Oceanic Technol.*, *19*, 738–746.
Weissman, D. E., B. W. Stiles, S. M. Hristova-Veleva, D. G. Long, D. K. Smith, K. A. Hilburn, and W. L. Jones (2012), Challenges to satellite sensors of ocean winds: Addressing precipitation effects, *J. Atmos. Oceanic Technol.*, *29*, 356–374, doi: 10.1175/JTECH-D-11-00054.1.
Yu, L., X. Jin, and R. Weller (2008), Multidecade global flux datasets from the Objectively Analyzed Air-sea Fluxes (OAFlux) project: Latent and sensible heat fluxes, ocean evaporation, and related surface meteorological variables. OAFlux Project Tech. Rep. OA-2008-01, 64 pp., Woods Hole, Mass. [Available at http://oaflux.whoi.edu/pdfs/OAFlux_TechReport_3rd_release.pdf.]
Yu, L., and X. Jin (2012), Buoy perspective of a high-resolution global ocean vector wind analysis constructed from passive radiometers and active scatterometers (1987-present), *J. Geophys. Res.*, *117*, C11013, doi:10.1029/2012JC008069.
Yu, L., and X. Jin (2014), Insights on the OAFlux ocean surface vector wind analysis merged from scatterometers and passive microwave radiometers (1987 onward), *J. Geophys. Res. Oceans*, *119*, 5244–5269, doi:10.1002/2013JC009648.
Yueh, S. H., B. W. Stiles, W.-Y. Tsai, H. Hu, and W. T. Liu (2001), QuikSCAT geophysical model function for tropical cyclones and applications to Hurricane Floyd, *IEEE Trans. Geosci. Remote Sens.*, *39*, 2601–2612.